

SCIENTIFIC REPORTS



OPEN

Revising of the Purcell effect in periodic metal-dielectric structures: the role of absorption

Konstantin M. Morozov^{1,2}, Konstantin A. Ivanov¹, Daniel de Sa Pereira³, Christopher Menelaou³, Andrew P. Monkman³, Galia Pozina⁴ & Mikhail A. Kaliteevski^{1,2,5}

Periodic metal-dielectric structures attract substantial interest since it was previously proposed that the spontaneous emission amplification rates (the Purcell factor) in such structures can reach enormous values up to 10^5 . However, the role of absorption in real metals has not been thoroughly considered. We provide a theoretical analysis showing that absorption leads to diminishing values of Purcell factor. We also suggest that using emitting organic compounds such as CBP (4,4-Bis(N-carbazolyl)-1,1-biphenyl) can lead to a moderate increase of about an order of magnitude in the Purcell factor. Defining the experimentally measured Purcell factor as a ratio between the excited state lifetimes in bare CBP and in periodic structure, this increase in the fabricated periodic structure is demonstrated through a 4–8 times decrease in excited state radiative lifetime compared to a bare organic material in a wide emission spectrum.

Recently, metallic nanostructures supporting plasmonic resonances have been attracting significant interest due to unique properties caused by a strong light-matter interaction^{1–4}. Surface plasmon (SP), which is a localized state of an electromagnetic field at the metal-dielectric interface, has been theoretically predicted more than half a century ago⁵. Localization of the electromagnetic field at metal-dielectric interfaces allows the implementation of various sub-wavelength optical devices^{6,7}, while the enhancement of the field's magnitude near the interface can be utilized for different sensing techniques^{8–11} and in novel applications based on plasmonic effects^{12–16}. The modification of the light-matter coupling can result in enhancement (Purcell effect)¹⁷ or in reduction of spontaneous emission rates which can improve the properties of light emitting of photovoltaic devices^{18–21}.

Recently, the giant value of the Purcell factor was suggested in periodic metal-dielectric structures^{22,23}. Also, it was proposed that a high spontaneous emission rate in such structures can be achieved through the high density of states (DOS), similar to the case of nanostructures with a high refractive index²⁴.

However, latter conclusions have been doubted²⁵ because in metals, absorption will hardly allow to utilize the benefits of the peculiar mode dispersion in the frequency range where the divergence in DOS happens for an ideal non-absorbing structure. Huge value of DOS associated with SP resonance is accompanied by absorption in plasma SP, which is not the case for all dielectric nanostructures²⁴. Furthermore, previous results²² were obtained using formalisms, which works only within the light cone for dielectric layers in metal-dielectric structures. However, the major contribution to DOS is provided by the regions of the phase space outside the light cone. At the same time, the idea to use peculiar mode dispersion in the periodic metal-dielectric structures²⁶ seems to be very compelling. Therefore, it is important and timely to provide a detailed analysis of the spontaneous emission rate in metal-dielectric structures taking into account absorption in metals and compare theoretical results with experimental studies.

Thus, in this work we study the influence of the absorption in metals on the modification of spontaneous emission in periodic metal-dielectric structures. To compare our model with the pre-existing model, where absorption in metals is neglected, we consider the structure identical to that analyzed by Iorsh *et al.*²².

¹ITMO University, 197101, St. Petersburg, Russia. ²St. Petersburg Academic University, 194021, St. Petersburg, Russia. ³Physics Department, Durham University, Durham, DH1 3LE, UK. ⁴Department of Physics, Chemistry and Biology (IFM), Linköping University, SE-58183, Linköping, Sweden. ⁵Ioffe Institute, 194021, St. Petersburg, Russia. Correspondence and requests for materials should be addressed to G.P. (email: galia.pozina@liu.se)

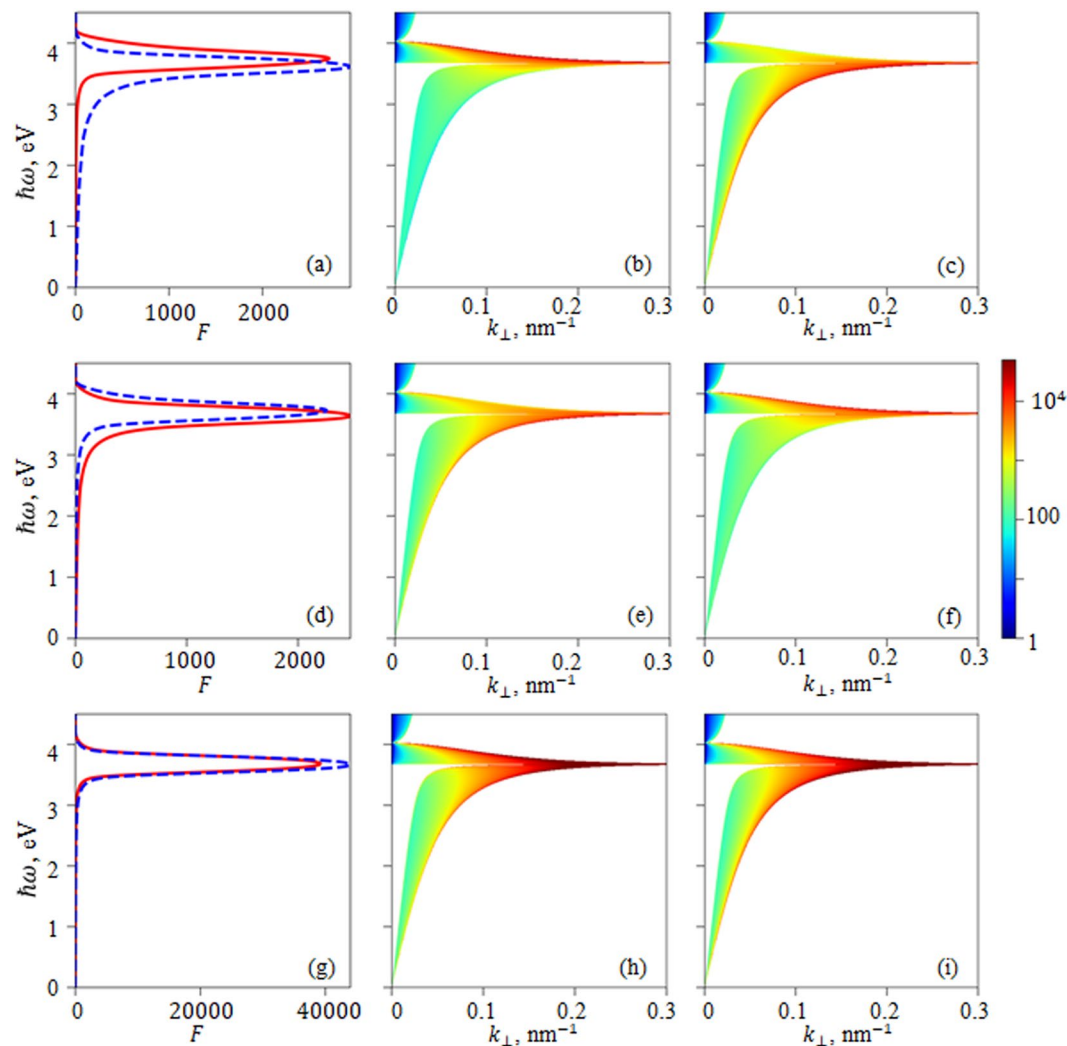


Figure 1. Integral Purcell factor (a,d,g) spontaneous emission probability density shown by color pattern (b,c,e,f,h,i) calculated for an infinite periodic structure of 15 nm Drude-modelled silver with no absorption/15 nm vacuum. The position of the emitting dipole is as follows: middle of the vacuum layer (top row); middle of the silver layer (middle row); layers interface (bottom row). Dipole orientation is as follows: parallel to the layers (red curve and middle column); perpendicular to the layers (blue curve and right column).

Results and Discussion

First, we have calculated the probability density of spontaneous emission for infinite idealized structures, for which we have assumed absence of absorption in silver. Such approximation is necessary for investigating of electromagnetic modes structure of infinite periodic structure. The period of the structure consisted of two layers: 15 nm of silver and 15 nm of vacuum. We limit our consideration to the case of TM polarization because SP and its associated features in the dispersion relations responsible for the increase of DOS and spontaneous emission rate can be realized only for TM polarization of light. The dispersion relations $\hbar\omega(K)$ and the spatial profile of the electromagnetic mode can be calculated using Bloch theorem (see chapter calculation technique of the section “Methods”). The resulting band structure is shown in Fig. 1. Plasmonic bands, positioned outside the light cone near the frequencies of SP of single silver-vacuum interface are clearly seen. SP and associated plasmonic band are waveguided modes, therefore, formally, there are solution for any wavevector k_{\perp} . At the same time, since concentration of electrons in the plasma is finite, we should confine the interval of wave vectors, which are considered by the value corresponding to the mean inverse distance between electrons in the plasma, which is about one third of inverse nanometer for silver. Based on the dispersion relation and the spatial profile of electromagnetic modes, one can calculate the probability density of spontaneous emission (Equation 10) for specific wavevector, and then, integrating it over k_{\perp} one can get the Purcell factor. Figure 1b,c,e,f,h,i show the dependence of the probability density on the wavevector k_{\perp} by color pattern. It can be seen, that major contributions to the Purcell factor is provided by the states with high values of k_{\perp} . Integrating the probability density of spontaneous emission, and normalizing it to the probability of the emission in the free space, one can obtain the Purcell factor, demonstrating pronounced peaks near the frequencies of SP on single interface.

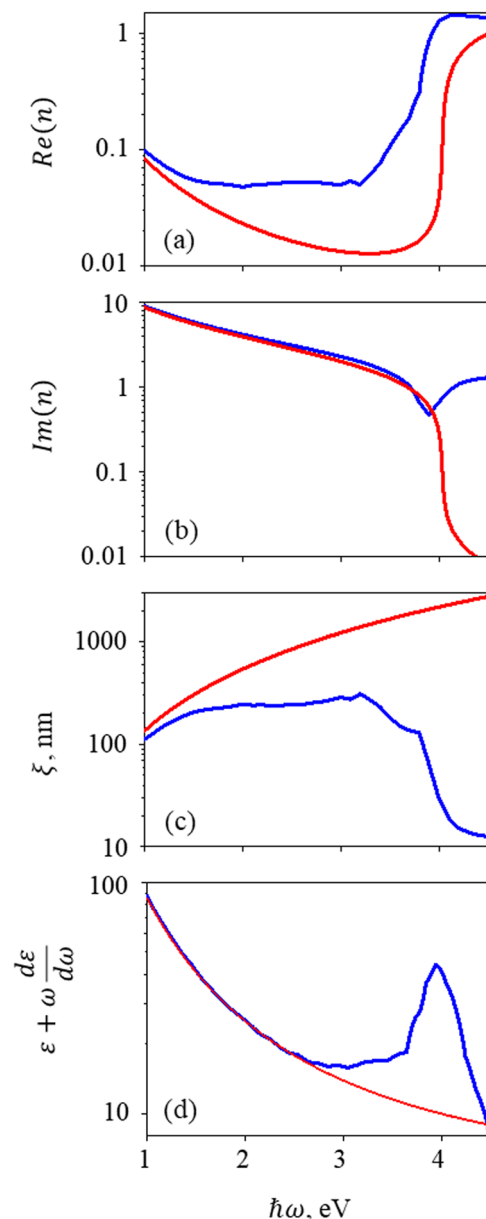


Figure 2. Real (a) and imaginary (b) parts of dielectric constant, coherence length (c) and energy density (d) for silver modelled according to the Drude theory with $\varepsilon_b = 4.96$, $\hbar\omega_p = 8.98$ eV and $\hbar\gamma = 0.018$ eV (red) and measured in experiment (blue).

To analyze the effect of absorption, we compare here results obtained for silver, which were used in our experimental studies and in previous theoretical work²².

The dielectric constant in metals according to the Drude theory can be written as follow:

$$\varepsilon_2 = \varepsilon_b - \frac{\omega_p^2}{\omega(\omega - i\gamma)} \quad (1)$$

Where for silver $\varepsilon_b = 4.96$, $\hbar\omega_p = 8.98$ eV and $\hbar\gamma = 0.018$ eV²⁷. However, the Drude theory fails within the frequency range which is particularly important for plasmon phenomena.

Figure 2 illustrates the comparison of the dielectric constant approximated by the Drude model with the dielectric constant measured experimentally for real silver²⁸. It is clear that the Drude model is inappropriate for the higher frequency range. The main difference is not related to the refractive index but to the definition of the coherence length:

$$\xi = \partial A / \partial z \quad (2)$$

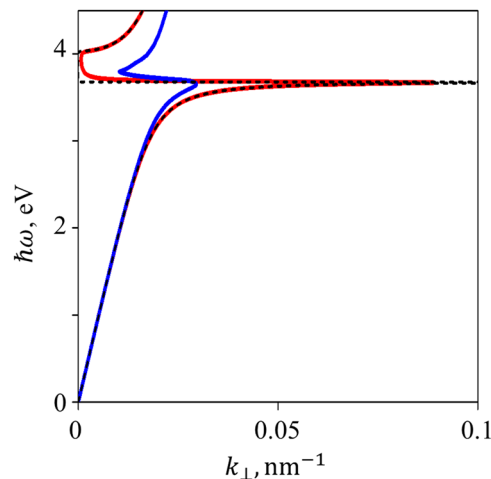


Figure 3. Plasmon dispersion for an interface between vacuum and silver modelled after the Drude theory without absorption consideration (black); with absorption consideration (red); for experimentally studied silver (blue).

Here A is the absorption coefficient. The coherence length for real silver is between 10 and 100 nm in the energy range of 3–4 eV. These values are much smaller than predicted by the Drude model, which leads to a significant reduction of any collective effects on scales beyond that length. Moreover, the energy density in metals is proportional to $\varepsilon + \omega d\varepsilon/d\omega$, whose value (plotted in Fig. 2d) differs dramatically for real silver.

The difference between the Drude model and experimental values becomes even more drastic for the plasmon dispersion curve. Indeed, from the dispersion equation we get the plasmon wavevector:

$$k_{\perp} = \frac{\omega}{c} \sqrt{\frac{\varepsilon_1 \varepsilon_2}{\varepsilon_1 + \varepsilon_2}} \quad (3)$$

Here ε_1 and ε_2 are dielectric constants of materials forming the interface. Comparison between a dispersion curve calculated using the Drude model and for real silver is shown in Fig. 3. We point out here that ignoring absorption in the Drude model leads to a situation when states with any wavevector k_{\perp} are available; at the same time, there is a forbidden zone for energy:

$$\omega_p / \sqrt{\varepsilon_1 + \varepsilon_b} < \omega < \omega_p / \sqrt{\varepsilon_b}.$$

The situation changes completely when absorption is taken into account. Now, the spectrum is continuous in the whole frequency range, but there is a limit on the values of the wavevector k_{\perp} . Numerically, its value doesn't exceed 0.1 nm^{-1} and 0.05 nm^{-1} for the Drude-modelled and experimentally measured silver, respectively.

For experimental structure, it is important to choose a suitable material that will serve as an emitter instead of vacuum layers. Currently, organic emitting materials are considered as very promising in the field of photonics²⁹. CBP (4,4-Bis(N-carbazolyl)-1,1-biphenyl) is one of the most popular host materials for different types of organic light emitting diode (OLED) systems including thermally activated delayed fluorescence devices due to its relatively large band-gap and ambipolarity^{30,31}. We have chosen CBP as the dielectric emitting organic material due to the fact that the interface between CBP and silver allows SP within the CBP emission region (see Fig. 4a for the CBP refractive index, PL spectrum and molecular structure scheme; the calculated plasmonic band structure is shown in Fig. 4b). Co-occurrence of the spectral position of the SP on the silver/CBP interface and the emission band of CBP could be used for development of efficient organic light-emitting diodes for the ultraviolet region.

It should be noted that attempts to use organic compounds as light emitters in periodic structures have been reported previously, however, without success in achieving high values of the Purcell factor³². The possible reason for this result can be related to the fact that the emitting material was only deposited on the surface of the structure. Contrary, we use an emitting organic material as the dielectric layer in each period of the structure.

Moreover, theoretical calculations of the Purcell factor for a single metal-dielectric interface have been performed for three different configurations: vacuum/silver (according to the Drude model), vacuum/silver (after experimental work)²⁸ and, finally, for CBP/silver (after experimental work)²⁸. The results are presented in Fig. 5. It can be seen that calculations with real silver accounts for a dramatic decrease in the Purcell factor (by more than two orders of magnitude), while using CBP has several effects such as a shift of the peak amplification away from a small coherence length region, an increase of the Purcell factor value to about 10 and broadening the spectrum.

In order to approve our theoretical analysis, we have fabricated a series of test structures with the different CBP layer thicknesses (10 nm, 15 nm, 20 nm and 30 nm) and with a silver layer with a thickness of 15 nm deposited on Al_2O_3 (sapphire) substrate (see Fig. 6a illustrating an example of the test structure). Cross-section scanning electronic microscopy (SEM) image of the 5 period 30 nm CBP/15 nm Ag is shown in Fig. 6b. To get SEM images, the sample was cracked, which affected interfaces; however, it is clear that the interfaces between CBP and silver achieved by this fabrication method are rather smooth.

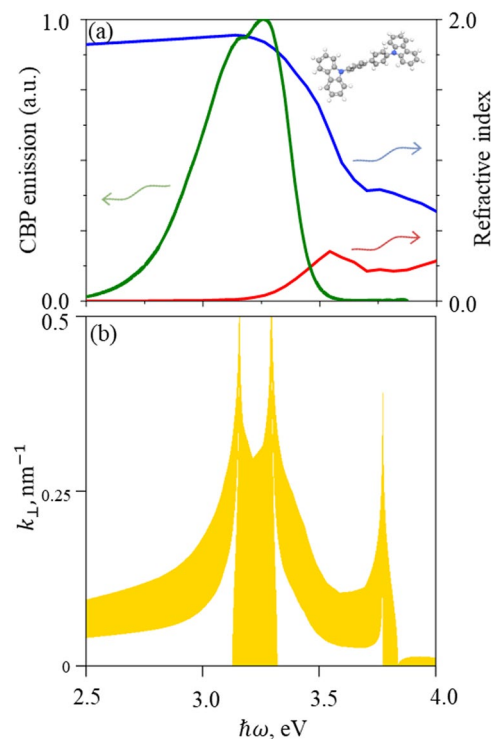


Figure 4. (a) Real (blue) and imaginary (red) parts of CBP's refractive index; PL spectrum of CBP (green). Inset shows molecular structure of CBP. (b) Plasmonic band structure for an infinite structure of 15 nm CBP/15 nm silver (band allowed for surface plasmon marked yellow).

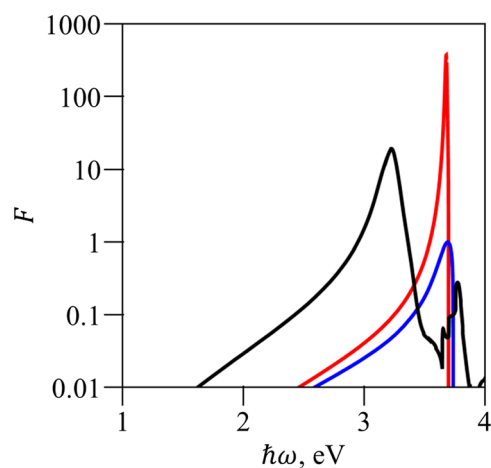


Figure 5. Purcell factor calculated for the interfaces between various materials: the Drude-modelled silver/vacuum (red); experimentally observed silver/vacuum (blue); experimentally observed silver/CBP (black). The emitter is placed at the interface and oriented parallel to it.

Room temperature photoluminescence spectra measured from the top of the aforementioned structure are presented in Fig. 7. The bare CBP layer shows a wide emission band in the frequency interval from 2.8 eV to 3.3 eV, and the emission spectrum almost does not depend on the emission angle. It can be seen that a periodic structure exhibits a trend of widening of the emission range compared to the bare emitting CBP while also growing distinct peaks which roughly correspond to plasmonic peaks in Fig. 4b. The positions of the basis peaks for different widths of CBP are nearly the same as in the bare CBP case (3.02 eV, 3.17 eV, 3.26 eV) but with a redistributed intensity according to the coupling with periodic structure.

Further, we measured the lifetimes of excited states at certain energies. Fluorescence decay of CBP material is determined by two lifetimes and biexponential behavior as shown in Fig. 8—an example of intensity decay curve for 20 nm CBP/15 nm Ag structure. The CBP molecule is characterized by “fast” ($\tau_{fast} \approx 0.33$ ns) and “slow”

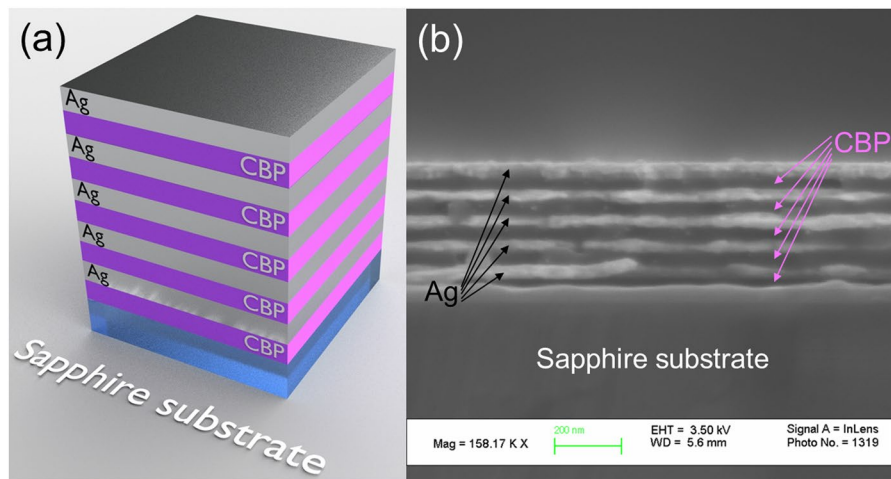


Figure 6. (a) Schematic drawing of the periodic CBP/Ag structure. (b) Cross-section SEM image of the 30 nm CBP/15 nm Ag structure at the sapphire substrate.

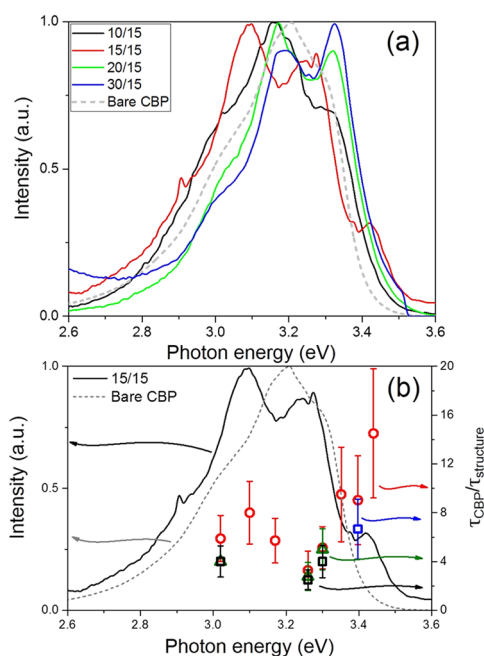


Figure 7. (a) PL spectra of the periodic structures with different CBP thicknesses in periodic samples: black curve ($d_{CBP} = 10$ nm), red curve ($d_{CBP} = 15$ nm), green curve ($d_{CBP} = 20$ nm) and blue curve ($d_{CBP} = 30$ nm). Dashed gray curve shows PL spectrum of the 50 nm bare CBP layer. (b) Ratios between lifetime of the CBP excited state in the bare CBP layer (τ_{CBP}) and lifetime in the periodic structure ($\tau_{structure}$). Black squares show the ratios for the 10 nm CBP/15 nm Ag structure. Red circles show the ratios for the 15 nm CBP/15 nm Ag structure and olive triangles show the ratios for 20 nm CBP/15 nm Ag structure case. Blue square shows the ratio for the 30 nm CBP/15 nm Ag structure. Solid black curve demonstrates PL spectrum of the 15 nm CBP/15 nm Ag structure.

($\tau_{slow} \approx 2$ ns) lifetimes and those parameters are constant within the error of measurement and approximation within the whole CBP emission range.

We define the experimentally measured Purcell factor as a ratio between the excited state lifetimes in bare CBP and in the periodic structure. In our case measurements showed that for every structure the ratios between “fast” lifetimes of a bare CBP and periodic structure are the same as the ratios between “slow” lifetimes within the range of the experimental error. Figure 7b demonstrates the distribution of lifetime ratios for various periodic structures at the energies corresponding to CBP emission range. Lifetime ratios’ magnitude is from 4 to 8; relatively high experimental error, especially at the edge of the CBP is due to low intensity of CBP emission at energies

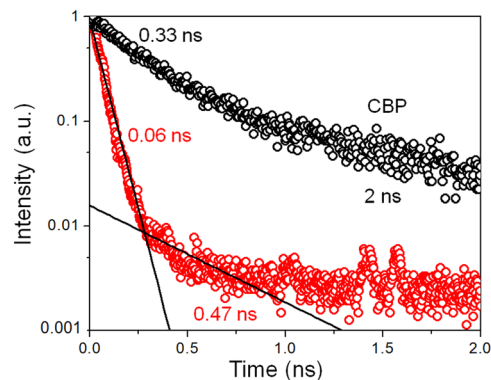


Figure 8. TCSPC measurements. PL decay time of bare CBP (black circles) and of periodic 20 nm CBP/15 nm Ag structure (red circles) taken at photon energy of 3.02 eV.

higher than 3.4 eV. This means moderate increase of spontaneous emission rate for the whole set of test structures. The interface between metal and CBP accounts for the majority of the decay, making it non-radiative. Taking this fact into account we can conclude that decrease in the excited state lifetime due to radiative decay in structures with various CBP thickness is still no less than 4.

Conclusions

In summary, we have modelled, fabricated and studied periodic metal-dielectric structures. We have shown that contrary to previous propositions the giant values of the calculated Purcell factor are only achievable when absorption in metals is not considered. Using experimentally obtained refractive index spectra for silver we have calculated that in a silver/vacuum structure the values can barely exceed unity. However, by tuning away from high DOS region and using organic materials that emit light in the plasmonic band one can achieve a moderate increase in the Purcell factor that is about 10 times higher than in simple metal/vacuum model. We have backed this claim with experimental study of a periodic structure that had CBP as active region. We have found that the excited state lifetime is 4–8 times shorter in metallic structures compared to bare CBP.

Methods

Sample preparation. The set of periodic structure samples with different thickness of the CBP (10 nm, 15 nm, 20 nm and 30 nm) was fabricated using a Kurt J. Lesker[®] Spectros II[™] system, an organic and metal thin film deposition system capable of reaching vacuum levels as low as 1×10^{-6} mbar. 5 periods of CBP and silver layers were deposited on the Al_2O_3 (sapphire) substrate. A set of calibration depositions for both materials was performed with greater accuracy. Also, a CBP layer of thickness 50 nm was grown on Al_2O_3 substrate for comparison of bare CBP properties with periodic structures properties.

Optical measurements. Emission spectra of bare CBP layer and periodical structures were measured using a Jobin-Yvon Horiba[®] Fluorolog[™] FL3-22 spectrometer (bare CBP and periodical structures were excited at 4.73 eV) at room temperature and atmospheric pressure.

Time-resolved measurements were performed using time-correlated single photon counting (TCSPC) measurement scheme at room temperature and atmospheric pressure. Structures were excited through the top silver layer at 262 nm wavelength, the third harmonic of the output from a Coherent[®] Mira[™] 900F Ti:Sapphire oscillator tuned to 786 nm central wavelength, with a 76 MHz repetition rate. A 365 ± 10 nm bandpass filter with OD (optical density) >4 outside this region was used. Samples were excited at 45° angle to the substrate normal. Emission from samples was collected also at 45° angle to the substrate normal at various energies (from 3.02 eV to 3.4 eV which is inside the range of CBP molecule emission).

Calculation techniques. To obtain the Purcell factor we start with deriving a formula for the emission probability. In an infinite structure with layers parallel to xy plane the coordinates in the k -vector space are (k_x, k_y, K) , where K is the Bloch vector. The well-known equation for the emission probability is:

$$dW = \frac{2\pi}{\hbar} |V_{fi}|^2 \delta(E_i - E_f - \hbar\omega) d\nu, \quad (4)$$

where dW is the probability of a radiative transition between dipole states with energies E_i and E_f . The transition is characterized by the matrix element V_{fi} , the photon energy $\hbar\omega$ and the number of photon states $d\nu$ that is proportional to a volume element in k -space and quantization volume V (which in an infinite structure spans one period):

$$d\nu = V \frac{dk_x dk_y dK}{(2\pi)^3}. \quad (5)$$

Since we are deriving the frequency Purcell factor we have to calculate $\int dW$ for a constant ω and then divide the obtained emission probability by that of a free space (where d is the absolute value of the dipole moment):

$$W_0 = \frac{2\omega^3 n}{3c^3 \hbar} |d|^2. \quad (6)$$

This task is approached by replacing variables (k_x, k_y, K) with $(\omega, k_\perp, \varphi)$ where k_\perp is the value of wavevector in xy plane and φ is the angle in this plane. This gives

$$d\nu = \frac{V}{(2\pi)^3} \left| \frac{dK}{d\omega} \right| k_\perp d\omega dk_\perp d\varphi. \quad (7)$$

At this point it is important to consider the matrix element V_{fi} :

$$V_{fi} = \mathbf{e}d\langle f|E|i \rangle \approx d \mathbf{e}rE(z_0) \quad (8)$$

Here we have assumed that the wavefunctions of initial and final states of the dipole overlap considerably only near the dipole position, z_0 . The values \mathbf{e} and \mathbf{r} are unit vectors of the electric field polarization and dipole orientation, respectively.

Both Equation 5 and Equation 7 reflect ambiguity in choosing the volume V because the number of states and the field amplitude depend on it; however, when the normalizing condition for the electric field amplitude

$$\frac{1}{4\pi} \int n(\mathbf{r})^2 |E(\mathbf{r})|^2 dV = \frac{\hbar\omega}{2} \quad (9)$$

is taken into account, we can part with V and postulate $V \equiv 1$ without it affecting the general derivation.

Substituting Equation 7 into Equation 4 and integrating over ω and φ , we get

$$dW_\omega(k_\perp) = \omega |d|^2 \frac{(\mathbf{e}r)^2 |E(z_0)|^2}{2\pi\hbar} \left| \frac{dK}{d\omega} \right| k_\perp dk_\perp. \quad (10)$$

Finally, using Equation 6 we get the integral Purcell factor:

$$F(\omega) = \frac{\int dW_\omega(k_\perp)}{W_0} = \frac{3c^3}{4\pi\omega^2} \int (\mathbf{e}r)^2 |E(z_0)|^2 \left| \frac{dK}{d\omega} \right| k_\perp dk_\perp. \quad (11)$$

In a finite structure such as a single interface, the procedure is very similar to the described above; however, we now deal with two dimensional k space, and after proper substitutions we obtain

$$d\nu = \frac{S}{(2\pi)^2} \left| \frac{dk_\perp}{d\omega} \right| k_\perp d\omega d\varphi \quad (12)$$

Here S is quantization space (as opposed to quantization volume). Then, the normalization condition can be expressed as follow:

$$\frac{S}{4\pi} \int_{-\infty}^{\infty} n(z)^2 |E(z)|^2 dz = \frac{\hbar\omega}{2} \quad (13)$$

after that the ambiguity in choosing S is also resolved. Finally, the value of Purcell factor is

$$F(\omega) = \frac{3\pi c^2}{\omega} k_\perp(\omega) \left| \frac{dk_\perp}{d\omega} \right| (\mathbf{e}r)^2 |E(z_0)|^2. \quad (14)$$

Data Availability

The experimental and modelling data are present in the paper. Additional data related to this paper may be requested from the authors.

References

1. Maier, S. A. *Plasmonics: fundamentals and applications*. Springer Science & Business Media (2007).
2. Zayats, A. V., Smolyaninov, I. I. & Maradudin, A. A. Nano-optics of surface plasmon polaritons. *Physics Reports* **408**, 131–314 (2005).
3. Pendry, J. B., Martin-Moreno, L. & Garcia-Vidal, F. J. Mimicking surface plasmons with structured surfaces. *Science* **305**, 847–848 (2004).
4. Schuller, J. A. *et al.* Plasmonics for extreme light concentration and manipulation. *Nat. Materials* **9**, 193–204 (2010).
5. Ritchie, R. H. Plasma losses by fast electrons in thin films. *Phys. Rev.* **106**, 874–881 (1957).
6. Barnes, W. L., Dereux, A. & Ebbesen, T. W. Surface plasmon subwavelength optics. *Nature* **424**, 824–830 (2003).
7. Ebbesen, T. W., Lezec, H. J., Ghaemi, H. F., Thio, T. & Wolff, P. A. Extraordinary optical transmission through sub-wavelength hole arrays. *Nature* **391**, 667–669 (1998).
8. Kumar, G., Sarswat, P. K. Interaction of surface plasmon polaritons with nanomaterials. *Reviews in Plasmonics*, Springer International Publishing, 103–129 (2016).
9. Yu, C. & Irudayaraj, J. Multiplex biosensor using gold nanorods. *Analyt. Chemistry* **79**, 572–579 (2007).

10. Baryshev, A. V. & Merzlikin, A. M. Approach to visualization of and optical sensing by Bloch surface waves in noble or base metal-based plasmonic photonic crystal slabs. *Appl. Optics* **53**, 3142 (2014).
11. Brolo, A. G. Plasmonics for future biosensors. *Nat. Photonics* **6**, 709–713 (2012).
12. Bellessa, J. *et al.* Giant Rabi splitting between localized mixed plasmon-exciton states in a two-dimensional array of nanosize metallic disks in an organic semiconductor. *Phys. Rev. B* **80**, 033303 (2009).
13. Ding, K. *et al.* Record performance of electrical injection sub-wavelength metallic-cavity semiconductor lasers at room temperature. *Optics Express* **21**, 4728 (2013).
14. Gubaydullin, A. R. *et al.* Enhancement of spontaneous emission in Tamm plasmon structures. *Sci. Reports* **7**, 9014 (2017).
15. Schlather, A. E., Large, N., Urban, A. S., Nordlander, P. & Halas, N. J. Near-field mediated plexcitonic coupling and giant Rabi splitting in individual metallic dimers. *Nano Letters* **13**, 3281–3286 (2013).
16. Song, J.-H. *et al.* Fast and bright spontaneous emission of Er³⁺ ions in metallic nanocavity. *Nat. Commun.* **6**, 7080 (2015).
17. Purcell, E. M., Torrey, H. C. & Pound, R. V. Resonance absorption by nuclear magnetic moments in a solid. *Phys. Rev.* **69**, 37–38 (1946).
18. Bykov, V. P. Spontaneous emission in a periodic structure. *Soviet J. Exper. Theor. Physics* **35**, 269 (1972).
19. Yablonovitch, E. Inhibited spontaneous emission in solid-state physics and electronics. *Phys. Rev. Lett.* **58**, 2059 (1987).
20. Huang, W. Q., Xu, L. & Wuet, K. Y. Enhancement of photoluminescence emission in low-dimensional structures formed by irradiation of laser. *J. Appl. Phys.* **102**, 053517 (2007).
21. Huang, W. Q., Liu, S. R., Huang, Z. M., Wu, X. K. & Qin, C. J. Localized states and quantum effect of photo-generated carriers in photovoltaic system. *Sci. Reports* **7**, 7221 (2017).
22. Iorsh, I., Poddubny, A., Orlov, A., Belov, P. & Kivshar, Y. S. Spontaneous emission enhancement in metal–dielectric metamaterials. *Phys. Lett. A* **376**, 185–187 (2012).
23. Poddubny, A., Iorsh, I., Belov, P. & Kivshar, Y. Hyperbolic metamaterials. *Nat. Photonics* **7**, 948–957 (2013).
24. Albella, P. *et al.* Low-loss electric and magnetic field-enhanced spectroscopy with subwavelength silicon dimers. *J. Phys. Chem. C* **117**, 13573–13584 (2013).
25. Khurgin, J. B. How to deal with the loss in plasmonics and metamaterials. *Nat. Nanotechnology* **10**, 2–6 (2015).
26. Vinogradov, A. P., Dorofeenko, A. V. & Nechepurenko, I. A. Analysis of plasmonic Bloch waves and band structures of 1D plasmonic photonic crystals. *Metamaterials* **4**, 181–200 (2010).
27. Johnson, P. B. & Christy, R. W. Optical Constants of the Noble Metals. *Phys. Rev. B* **6**, 4370–4379 (1972).
28. Babar, S. & Weaver, J. H. Optical constants of Cu, Ag, and Au revisited. *Appl. Optics* **54**, 477 (2015).
29. Kamtekar, K. T., Monkman, A. P. & Bryce, M. R. Recent advances in white organic light-emitting materials and devices (WOLEDs). *Adv. Materials* **22**, 572–582 (2010).
30. Dias, F. B. *et al.* The role of local triplet excited states and D–A relative orientation in thermally activated delayed fluorescence: photophysics and devices. *Adv. Science* **3**, 1600080 (2016).
31. Jankus, V., Winscom, C. & Monkman, A. P. The photophysics of singlet, triplet, and degradation trap states in 4,4-N,N'-dicarbazolyl-1,1'-biphenyl. *J. Chem. Phys.* **130**, 074501 (2009).
32. Tsurumachi, N. *et al.* Dependence of Purcell effect on fluorescence wavelength in dye molecules on metal–dielectric multilayer hyperbolic metamaterials. *Jap. J. Appl. Phys.* **55**, 02BB05 (2016).

Acknowledgements

K.M.M., K.A.I. and M.A.K. acknowledge the support from the Russian Science Foundation, grant #16-12-10503, G.P. acknowledge the Swedish Energy Agency.

Author Contributions

M.A.K. designed the research idea. K.M.M., D.d.S.P., C.M. and A.P.M. fabricated and performed TCSPC and spectral measurements of the test structure. G.P. contributed to SEM measurements. K.A.I. and M.A.K. conducted the analysis and calculations. Authors contributed equally to the discussion of the results. K.M.M., K.A.I., G.P. and M.A.K. wrote the manuscript with contribution from all authors.

Additional Information

Competing Interests: The authors declare no competing interests.

Publisher's note: Springer Nature remains neutral with regard to jurisdictional claims in published maps and institutional affiliations.



Open Access This article is licensed under a Creative Commons Attribution 4.0 International License, which permits use, sharing, adaptation, distribution and reproduction in any medium or format, as long as you give appropriate credit to the original author(s) and the source, provide a link to the Creative Commons license, and indicate if changes were made. The images or other third party material in this article are included in the article's Creative Commons license, unless indicated otherwise in a credit line to the material. If material is not included in the article's Creative Commons license and your intended use is not permitted by statutory regulation or exceeds the permitted use, you will need to obtain permission directly from the copyright holder. To view a copy of this license, visit <http://creativecommons.org/licenses/by/4.0/>.

© The Author(s) 2019